Astronomy & Astrophysics manuscript no. vudsXELGs˙arxiv
March 18, 2014

Letter to the Editor

Discovering extremely compact and metal-poor, star-forming dwarf galaxies out to $z \sim 0.9$ in the VIMOS Ultra-Deep Survey⋆

R. Amorín[1], V. Sommariva[5,1], M. Castellano[1], A. Grazian[1], L. A. M. Tasca[2], A. Fontana[1], L. Pentericci[1], P. Cassata[2], B. Garilli[4], V. Le Brun[2], O. Le Fèvre[2], D. Maccagni[4], R. Thomas[2], E. Vanzella[3], G. Zamorani[3], E. Zucca[3], S. Bardelli[3], P. Capak[12], L. Cassará[4], A. Cimatti[5], J.G. Cuby[2], O. Cucciati[5,3], S. de la Torre[2], A. Durkalec[2], M. Giavalisco[13], N. P. Hathi[2], O. Ilbert[2], B. C. Lemaux[2], C. Moreau[2], S. Paltani[9], B. Ribeiro[2], M. Salvato[14], D. Schaerer[10,8], M. Scodeggio[4], M. Talia[5], Y. Taniguchi[15], L. Tresse[2], D. Vergani[6,3], P.W. Wang[2], S. Charlot[7], T. Contini[8], S. Fotopoulou[9], C. López-Sanjuan[11], Y. Mellier[7], and N. Scoville[12]

(Affiliations can be found after the references)

ABSTRACT

We report the discovery of 31 low-luminosity ($-14.5 \gtrsim M_{AB}(B) \gtrsim -18.8$), extreme emission line galaxies (EELGs) at $0.3 \lesssim z \lesssim 0.9$ identified by their unusually high rest-frame equivalent widths (100< EW[O III] <1700Å) as part of the VIMOS Ultra Deep Survey (VUDS). VIMOS optical spectra of unprecedented sensitivity ($I_{AB} \sim 25$ mag) along with multiwavelength photometry and HST imaging are used to investigate spectrophotometric properties of this unique sample and explore, for the first time, the very low stellar mass end ($M_\star \lesssim 10^8\,M_\odot$) of the luminosity-metallicity (LZR) and mass-metallicity (MZR) relations at $z < 1$. Characterized by their extreme compactness ($R_{50} < 1$ kpc), low stellar mass and enhanced specific star formation rates ($SFR/M_\star \sim 10^{-9}$-10^{-7}yr^{-1}), the VUDS EELGs are blue dwarf galaxies likely experiencing the first stages of a vigorous galaxy-wide starburst. Using T_e-sensitive *direct* and strong-line methods, we find that VUDS EELGs are low-metallicity ($7.5 \lesssim 12+\log(O/H) \lesssim 8.3$) galaxies with high ionization conditions i.e. $\langle O\,III/O\,II\rangle = 4 \pm 5$. Moreover, we find at least three objects showing HeIIλ 4686Å emission and four EELGs of extremely low metallicities (≲10% solar). The LZR and MZR followed by EELGs are broadly consistent with the extrapolation toward low mass of these relations from previous studies at similar redshift. However, we find evidences that galaxies with younger and more vigorous star formation – as characterized by their larger Hβ and [O III] EWs, sSFR and higher ionization parameters – tend to be more metal-poor at a given luminosity and stellar mass. These results are discussed in the context of the fundamental metallicity relation linking mass metallicity and SFR.

Key words. galaxies : evolution – galaxies : high redshift – galaxies : dwarfs – galaxies : abundances – galaxies : starbursts

1. Introduction

Over the last 8 billion years a large fraction of low-mass ($M_\star \lesssim 10^9\,M_\odot$) galaxies are still seen rapidly assembling most of their present-day stellar mass (Cowie et al. 1996; Pérez-González et al. 2008). Tracing the spectrophotometric properties of these vigorous star-forming *dwarf* galaxies (SFDGs) out to $z \sim 1$ is essential not only to study how they evolve through cosmic time, but also to understand the physical mechanisms driving the first stages of stellar mass build-up and chemical enrichment. To this end, key insights can be obtained from the tight relations found between stellar mass, metallicity and star formation rate (SFR). However, the shape and normalization of these relations at different redshifts are still poorly constrained at their low-mass end. While in the local Universe the mass-metallicity relation (MZR) has been extended down to $10^8\,M_\odot$ (e.g. Andrews & Martini 2013), at intermediate and high redshifts, dwarf galaxies are strongly under-represented (e.g. Henry et al. 2013).

These SFDGs are usually identified by their blue colors, high surface brightness and strong emission-lines. They include a rare population of extreme emission-line galaxies (EELGs) with the largest nebular content and lowest metal abundances (e.g. Kniazev et al. 2004; Papaderos et al. 2008; Hu et al. 2009; Atek et al. 2011; Morales-Luis et al. 2011). Due to their high equivalent widths (EWs), an increasing number of EELGs are being dicovered and characterized by deep spectroscopic surveys out to $z \sim 1$ (e.g. Hoyos et al. 2005; Ly et al. 2014; Amorín et al. 2014a) and beyond (e.g. van der Wel et al. 2011; Maseda et al. 2014). In this *Letter* we report the discovery of a sample of 31 EELGs at $0.2 \lesssim z \lesssim 0.9$ identified from the *VIMOS Ultra-Deep Survey* (VUDS; Le Fèvre et al. 2014). We study their physical properties as part of a larger, ongoing study aimed at investigating the evolution of SFDGs out to $z \sim 1$ using very deep spectroscopy (e.g. Amorín et al. 2014a). The sensitivity of our VUDS spectra, detecting emission lines as faint as $\sim 1.5\times10^{-18}$ erg s^{-1} cm^{-2}, makes it possible to derive T_e-based metallicities for a fraction of such faint galaxies. Thus, the present sample extends previous studies of star-forming galaxies at similar redshifts in size and limiting magnitude (Henry et al. 2013; Ly et al. 2014), allowing to study, in larger detail, the LZR and MZR at $z < 1$ two decades below $10^9 M_\odot$ with galaxies showing a wide range of properties, including a number of extremely metal-poor galaxies ($Z < 0.1 Z_\odot$). Throughout this paper we adopt a standard Λ-CDM cosmology with $h = 0.7$, $\Omega_m = 0.3$ and $\Omega_\Lambda = 0.7$.

Send offprint requests to: R. Amorín e-mail: ricardo.amorin@oa-roma.inaf.it

⋆ Based on data obtained with the European Southern Observatory Very Large Telescope, Paranal, Chile, under Large Program 185.A-0791.

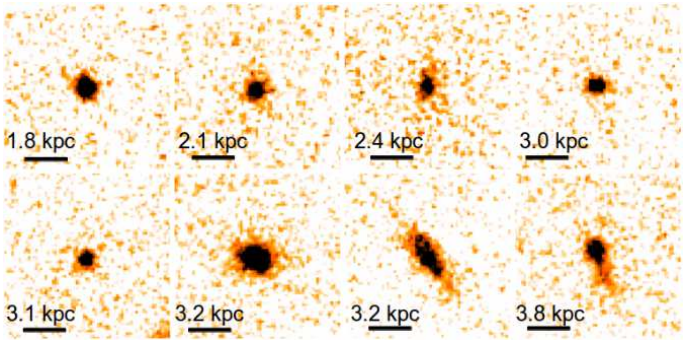

Fig. 1. HST $F814W$-band imagery of EELGs in the COSMOS and ECDF fields covered by VUDS. Each postage stamp is 2" on a side.

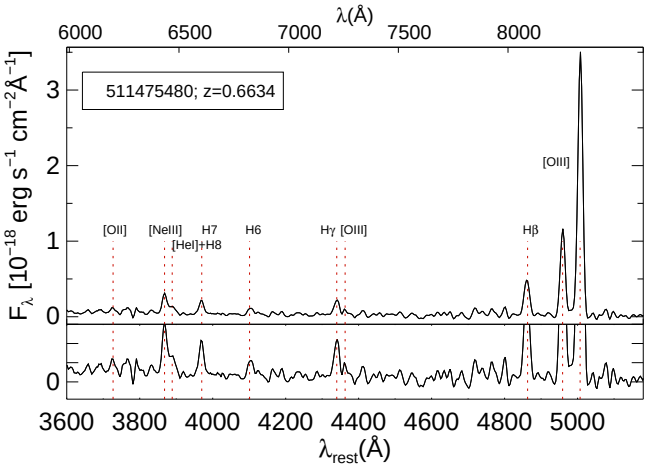

Fig. 2. Deep VIMOS spectrum of a high ionization, extremely metal-poor ($Z \sim 0.07\,Z_\odot$) EELG in VUDS. A zoomed version is shown in the bottom panel. The main nebular emission lines are labelled.

2. Observations and sample selection

VUDS is a deep spectroscopic legacy survey of $\sim 10^4$ galaxies carried out using VIMOS at ESO-VLT (Le Fèvre et al. 2003). VUDS is aimed at providing a complete census of the star-forming galaxy population at $2 \lesssim z \lesssim 7$, covering $\sim 1\,\mathrm{deg}^2$ in three fields: COSMOS, ECDFS and VVDS-2h. The VIMOS spectra consist of 14h integrations in the LRBLUE and LRRED grism settings, respectively, covering a combined wavelength range $3650 < \lambda < 9350$Å, with a spectral resolution R∼230. Data reduction, redshift measurement and assessment of the reliability flags are described in detail in the survey and data presentation paper (Le Fèvre et al. 2014).

VUDS targets have been primarily selected to have photometric redshifts $z_p > 2.4$ for either of the primary and secondary peaks of the PDF. A number of random targets purely magnitude selected to $I_{\rm AB} \leq 25$ have been added to fill empty areas on observed slit masks. As a consequence, we identify a number of targets with spectroscopic redshift $z_s < 2$. Many of these targets are galaxies with prominent optical emission lines, such as [O II]λ3727 or [O III]λ5007, that artificially boost the observed magnitudes in the stellar spectral energy distributions (SED).

For this *Letter* a representative sample of 31 EELGs (12 from COSMOS, 11 from VVDS-2h and 8 from ECDFS) with mean $I_{\rm AB}$ ∼24.5 mag was identified from an early version of VUDS containing ∼40% of the final sample. We first consider primary and secondary target galaxies with very reliable spectroscopic redshift (98% and 100% confidence level), at $0.03 \lesssim z \lesssim 0.93$. We then select galaxies with at least three emission lines detected, [O II], [O III] and Hβ, and EW[O III]> 100Å. The first criterion ensures the derivation of gas-phase metallicities and the second one allow to select EELGs with the highest *specific* SFR (e.g. Atek et al. 2011; Ly et al. 2014; Amorín et al. 2014a).

While our EELGs look unresolved in ground-based images precluding a full morphological analysis, morphological information can be obtained for a subset of 16 EELGs that have been observed by the HST-ACS in the $F814W$ (I) band. As illustrated in Fig. 1, EELGs include galaxies with both round and irregular shapes, showing angular sizes < 1". Using the automated method presented in Tasca et al. (2009) for the EELGs imaged by the ACS we derive circularized half-light radii, $r_{50} = R_{50}\,(b/a)^{0.5} \sim 0.4$-$0.8$ kpc thus confirming their extreme compactness. In most cases, we find these EELGs with no clear signs of ongoing mergers or very close companions.

3. Physical properties of VUDS EELGs

In this section we describe the derivation of the main physical properties for the EELG sample and list the most relevant ones in Table 2, which is available in electronic form only. As shown in Fig. 2, our VUDS spectroscopy is extremely deep. While in many cases we can detect a remarkably faint continuum ($\sim 5\times10^{-20}$erg s^{-1} cm^2 Å, 1σ), very faint lines, such as [O III]λ4363, can be detected with good significance levels. Line fluxes and EWs and their uncertainties have been measured manually using the IRAF task *splot* following Amorín et al. (2012), and have been de-reddened using the Balmer decrement and the Calzetti et al. (2000) extinction law. The mean reddening of EELGs in VUDS is $\langle E(B-V)_{\rm gas}\rangle = 0.26\pm0.14$, in excellent agreement with previous studies for EELGs (e.g. Domínguez et al. 2013; Ly et al. 2014; Amorín et al. 2014a). In those cases where $E(B-V)_{\rm gas}$ cannot be measured through Hα/Hβ or Hβ/Hγ, we adopt $E(B-V)_{\rm gas} = E(B-V)_\star$, where $E(B-V)_\star$ is the stellar extinction derived from the SED fitting described in Section 3.2. This seems reasonable since median values of stellar ($\langle E(B-V)_\star\rangle = 0.25 \pm 0.14$) and gas extinctions are in excellent agreement for galaxies for which the both values are available.

3.1. Ionization and metallicity properties from VUDS spectra

In Figure 3 we study the ionization properties of the EELG sample using three diagnostic diagrams based on strong emission line ratios. Our sample galaxies populate the region of star-forming galaxies with the highest excitation ([O III]/Hβ∼ 5±2). Consistently with their low masses and blue $U-B$ colors, none of them shows indication of AGN activity. Our sample galaxies, however, are located near the limits between SF and AGN regions in Fig. 3 due to their high ionization conditions, as suggested by their high [O III]/[O II] ratios (Fig. 3a). In the most extreme cases, [O III] shows EWs of ~ 1700Å, while the [O II] line is only barely detected (e.g. Fig. 2). Moreover, in three EELGs, we tentatively detect (∼2.5σ) HeIIλ4686Å emission, suggesting the presence of very young, hot stars. Being rare at $z < 1$ (e.g. Jaskot & Oey 2013; Nakajima & Ouchi 2013; Amorín et al. 2014a), these EELGs show ionization parameters ($\log(q_{\rm ion}) \gtrsim 8\,\mathrm{cm\,s^{-1}}$) comparable to some low-luminosity high

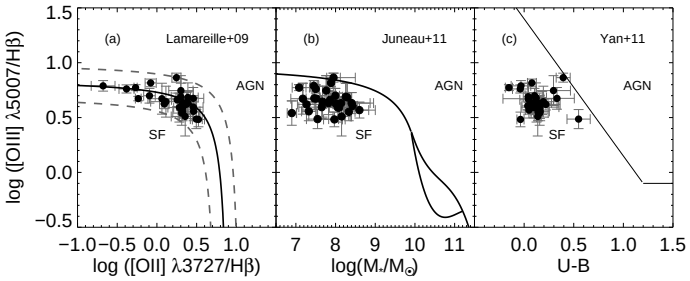

Fig. 3. Diagnostic diagrams. Lines show the empirical separations between star-forming (SF) galaxies and AGNs.

redshift galaxies (e.g. Fosbury et al. 2003; Amorín et al. 2014b).

In seven EELGs we detect ($\geq 3\sigma$) the intrinsically faint T_e−sensitive auroral line [O III]λ4363Å. For these galaxies we derive metallicity using the direct method (Hägele et al. 2008). In addition, we derive metallicities for the entire sample using the $R23(\equiv$(O II+O III)/Hβ) parameter and the calibration of McGaugh (1991). Following Pérez-Montero et al. (2013) we applied the linear relations detailed in Lamareille et al. (2006) to make these R23 metallicities consistent with those derived using the direct method. In order to break the degeneracy of $R23$ (i.e. to choose between the lower or upper branch) we use two additional indicators. For EELGs at $z \lesssim 0.45$ we choose the branch that best matches the metallicity obtained from the $N2(\equiv$N II/Hα) parameter and the calibration by Pérez-Montero & Contini (2009), while for EELGs at $z \gtrsim 0.45$ we choose the branch that best matches the metallicity from the calibrations based on the [Ne III], [O II] and [O III] line ratios of Maiolino et al. (2008). The difference between direct and strong-line metallicity estimations for the seven galaxies with [O III]λ4363Å is <0.2 dex. We find the metallicity of our EELG spanning a wide range of sub-solar values ($7.5\lesssim 12+\log(O/H)\lesssim 8.3$), including four extremely metal-poor galaxies ($Z \lesssim 0.1 Z_\odot$).

3.2. Stellar properties from multiwavelength SED fitting

Stellar masses and rest-frame absolute magnitudes of EELGs were derived by fitting their SEDs following Castellano et al. (2014). In short, we fit Bruzual & Charlot (2003) stellar population synthesis models to the broad-band photometry – from UV to NIR – of each galaxy using chi-square minimization. Following Amorín et al. (2014a), magnitudes are previously corrected from the contribution of prominent optical emission lines, while models assume stellar metallicities that best agree with the observed gas-phase metallicity. We adopt a Chabrier (2003) IMF, Calzetti et al. (2000) extinction law and assume a standard declining exponential star formation history. As a result, we find the sample of EELGs in VUDS spanning a range of low luminosities, $-14.5 \lesssim M_{\rm AB}(B) \lesssim -18.8$, and low stellar masses, $6.9 \lesssim \log(M_\star/M_\odot) \lesssim 8.6$.

4. The relation between mass, metallicity and ongoing SFR of low-mass galaxies out to $z \sim 1$

In Figure. 4 we show the SFR-mass diagram for the EELGs in VUDS and other EELGs from the literature. Star formation rates are derived from the extinction-corrected Hα or Hβ luminosities using the calibration of Kennicutt (1998) and assuming a Chabrier (2003) IMF. At a given redshift, our EELGs show

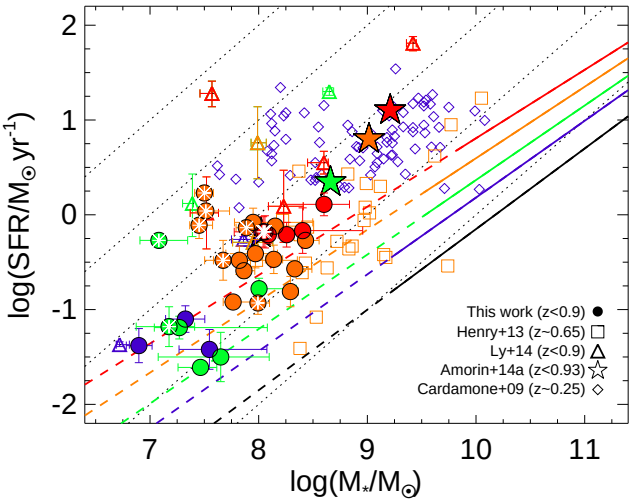

Fig. 4. The SFR stellar mass plane of low-mass SFDGs. Solid and dashed lines show the so-called 'main sequence' of galaxies at different redshifts and its extrapolation to low-mass regime, respectively, according to Whitaker et al. (2012). Dotted lines indicate constant sSFR from 10^{-10} yr^{-1} (bottom) to 10^{-6} yr^{-1} (upper). Colours indicate redshift bins with mean values $\langle z \rangle = 0$ (black), $\langle z \rangle = 0.25$ (blue), $\langle z \rangle = 0.4$ (green), $\langle z \rangle = 0.6$ (orange) and $\langle z \rangle = 0.8$ (red). Asterisks highlight VUDS EELGs with EW$_{\rm rest}$(O III) > 200Å and EW$_{\rm rest}$(Hβ) > 70Å.

SFRs and stellar masses a factor of ∼10 lower than similar samples from the literature, (cf. e.g. median EELG values in zCOSMOS; Amorín et al. 2014a, shown by stars). However, nearly all EELGs shown in Fig. 4 are well above the extrapolation to low stellar mass of the "main sequence" of galaxies (Whitaker et al. 2012) at a given z. The EELGs in VUDS show enhanced *specific* SFRs (sSFR$\sim 10^{-9}$-10^{-7} yr^{-1}) and SFR surface densities ($\Sigma_{\rm SFR}$ = SFR$/2\pi r_{50}^2$ ~ 0.35 (± 0.19) M$_\odot$ yr^{-1} kpc^{-2}), comparable to more luminous galaxy-wide starbursts at similar and higher redshifts (Ly et al. 2014; Amorín et al. 2014a,b).

In Figure 5 we study the LZR and MZR traced by EELGs in VUDS and other low-mass galaxies at $0 < z < 1$. The EELGs extents the LZR down to $M_{\rm AB}(B) \sim -14.5$ and the MZR down to M$_\star$ $\sim 10^7$M$_\odot$, which means ∼1 dex lower than previous studies (e.g. Henry et al. 2013), thus increasing substantially the number of low-mass galaxies under study, especially at $z \gtrsim 0.5$. Despite the relatively large scatter, VUDS EELGs appear to follow the LZR and MZR of more luminous and massive SFDGs. In particular, we find most EELGs in broad agreement with the local ($z < 0.3$) LZR of Guseva et al. (2009) and MZR of Andrews & Martini (2013), which have been derived from galaxies with measured electron temperatures. There is nevertheless a tendency for EELGs with larger EWs to be more metal-poor at a given luminosity and stellar mass, independently of redshift. These galaxies are those with the highest sSFR, i.e. those with the largest deviations from the "main sequence" of star formation at a given z, in Fig. 4. While in the LZR they follow better the LZR traced by extremely metal-poor galaxies (e.g. Kewley et al. 2007; Hu et al. 2009), they tend to lie below the local MZR, similarly to other extreme galaxies e.g., the *green peas*.

The above dependence of the MZR on SFR can be studied in the context of the fundamental metallicity relation (FMR; Mannucci et al. 2010), as shown in Fig. 5. While some EELGs do follow the FMR, some of the most extreme EELGs in terms

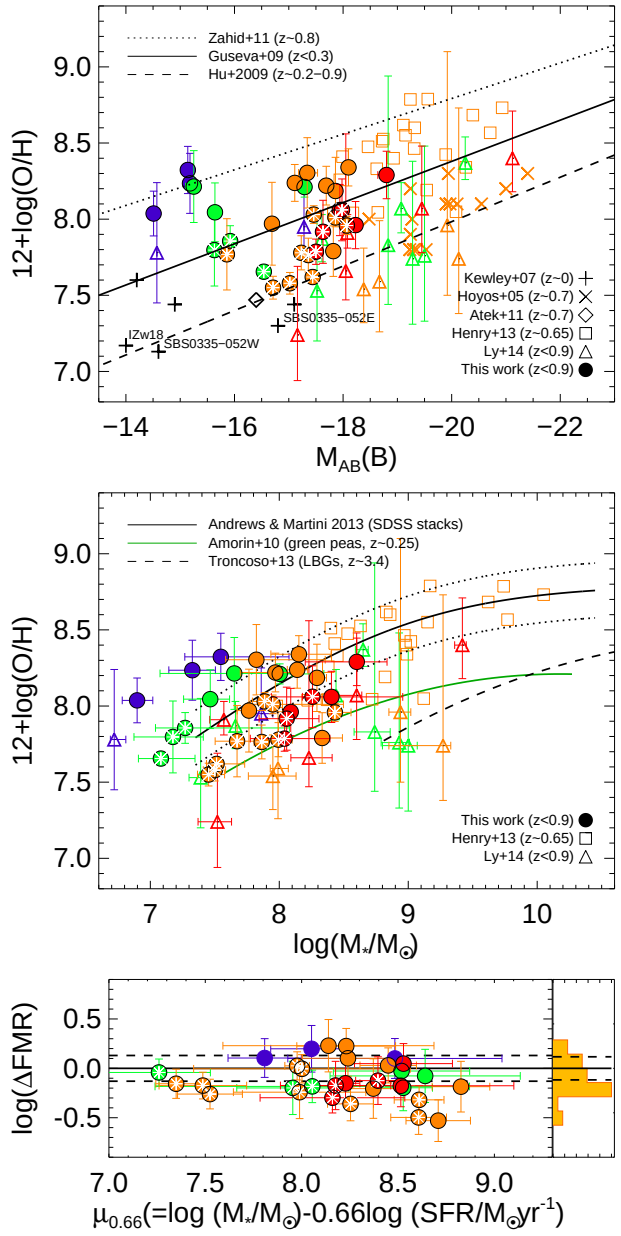

Fig. 5. *Upper and middle panels:* The luminosity-metallicity and stellar mass-metallicity relations for VUDS EELGs and SFDGs from the literature. *Lower panel:* Deviations from the FMR for VUDS EELGs (Andrews & Martini 2013). Colours and asterisks are as in Fig. 4. The data have been homogenized to the Chabrier (2003) IMF.

of EWs and sSFR tend to deviate >2σ to lower metallicities from the FMR traced by "main sequence" galaxies. These EELGs are most probably caught in an early stage of a galaxy-wide starburst. In addition to gas outflows – which are likely in such low-mass systems – these galaxies may still showing the effects of recent massive accretion of metal-poor gas, which feeds star formation and dilutes the oxygen abundances (e.g. Amorín et al. 2010; Sánchez Almeida et al. 2014; Troncoso et al. 2014).

Offsets like those observed in the MZR – which are usually found at low mass – also suggest that the shape of the MZR is very sensitive to selection effects in its very low-mass end. Starbursting dwarfs with enhanced EW and sSFR may be over-represented with respect to the global population of low-mass galaxies in spectroscopic samples at such faint luminosities, making the shape of the MZR at low mass not entirely representative of "main sequence" galaxies. Clearly, a thorough study using the deepest spectroscopy available for a statistical and representative sample of SFDGs is much needed to test this hypothesis. Forthcoming analysis of VUDS galaxies at $z < 1$ using the complete database will enable us to scrutinize in detail the under-explored low-mass universe at $z < 1$.

Acknowledgements. We thank ESO staff for their continuous support for the VUDS survey, particularly the Paranal staff conducting the observations and Marina Rejkuba and the ESO user support group in Garching. This work is supported by funding from the European Research Council Advanced Grant ERC-2010-AdG-268107-EARLY and by INAF Grants PRIN 2010, PRIN 2012 and PICS 2013. RA and AF acknowledge the FP7 SPACE project ASTRODEEP (Ref.No: 312725), supported by the European Commission. AC, OC, MT and VS acknowledge the grant MIUR PRIN 2010–2011. DM gratefully acknowledges LAM hospitality during the initial phases of the project. This work is based on data products made available at the CESAM data center, Laboratoire d'Astrophysique de Marseille. This work partly uses observations obtained with MegaPrime/MegaCam, a joint project of CFHT and CEA/DAPNIA, at the Canada-France-Hawaii Telescope (CFHT) which is operated by the National Research Council (NRC) of Canada, the Institut National des Sciences de l'Univers of the Centre National de la Recherche Scientifique (CNRS) of France, and the University of Hawaii. This work is based in part on data products produced at TERAPIX and the Canadian Astronomy Data Centre as part of the Canada-France-Hawaii Telescope Legacy Survey, a collaborative project of NRC and CNRS.

References

Amorín, R. O., Pérez-Montero, E., & Vílchez, J. M. 2010, ApJ, 715, L128
Amorín, R., Pérez-Montero, E., Vílchez, J. M., & Papaderos, P. 2012, ApJ, 749, 185
Amorín, R., Pérez-Montero, E., Contini, T., et al. 2014a, A&A, submitted
Amorín, R., Grazian, A., Castellano, M., et al. 2014b, ApJ, submitted
Andrews, B. H., & Martini, P. 2013, ApJ, 765, 140
Atek, H., Siana, B., Scarlata, C., et al. 2011, ApJ, 743, 121
Bruzual, G. & Charlot, S. 2003, MNRAS, 344, 1000
Calzetti, D., Armus, L., Bohlin, R. C., et al. 2000, ApJ, 533, 682
Cardamone, C., Schawinski, K., Sarzi, M., et al. 2009, MNRAS, 399, 1191
Castellano, M., et al. 2014, arXiv:1403.0743
Cowie, L. L., Songaila, A., Hu, E. M., & Cohen, J. G. 1996, AJ, 112, 839
Chabrier, G. 2003, PASP, 115, 763
Domínguez, A., Siana, B., Henry, A. L., et al. 2013, ApJ, 763, 145
Fosbury, R. A. E., Villar-Martín, M., Humphrey, A., et al. 2003, ApJ, 596, 797
Guseva, N. G., Papaderos, P., Meyer, H. T., Izotov, Y. I., & Fricke, K. J. 2009, A&A, 505, 63
Hägele, G. F., Díaz, Á. I., Terlevich, E., et al. 2008, MNRAS, 383, 209
Henry, A., Martin, C. L., Finlator, K., & Dressler, A. 2013, ApJ, 769, 148
Hoyos, C., Koo, D. C., Phillips, A. C., Willmer, C. N. A., & Guhathakurta, P. 2005, ApJ, 635, L21
Hu, E. M., Cowie, L. L., Kakazu, Y., & Barger, A. J. 2009, ApJ, 698, 2014
Jaskot, A. E., & Oey, M. S. 2013, ApJ, 766, 91
Juneau, S., Dickinson, M., Alexander, D. M., & Salim, S. 2011, ApJ, 736, 104
Kennicutt, R. C., Jr. 1998, ApJ, 498, 541
Kewley, L. J., Brown, W. R., Geller, M. J., Kenyon, S. J., & Kurtz, M. J. 2007, AJ, 133, 882
Kniazev, A. Y., Pustilnik, S. A., Grebel, E. K., Lee, H., & Pramskij, A. G. 2004, ApJS, 153, 429
Lamareille, F., Contini, T., Brinchmann, J., et al. 2006b, A&A, 448, 907
Lamareille, F., Brinchmann, J., Contini, T., et al. 2009, A&A, 495, 53
Le Fèvre, O., Saisse, M., Mancini, D., et al. 2003, Proc. SPIE, 4841, 1670
Le Fèvre, O., et al. 2014, A&A, submitted
Ly, C., Malkan, M. A., Nagao, T., et al. 2014, ApJ, 780, 122
Maiolino, R., Nagao, T., Grazian, A., et al. 2008, A&A, 488, 463
Mannucci, F., Cresci, G., Maiolino, R., Marconi, A., & Gnerucci, A. 2010, MNRAS, 408, 2115
Maseda, M., et al. ApJ, submitted
McGaugh, S. S. 1991, ApJ, 380, 140
Morales-Luis, A. B., Sánchez Almeida, J., Aguerri, J. A. L., & Muñoz-Tuñón, C. 2011, ApJ, 743, 77
Nakajima, K., & Ouchi, M. 2013, arXiv:1309.0207
Papaderos, P., Guseva, N. G., Izotov, Y. I., & Fricke, K. J. 2008, A&A, 491, 113
Pérez-Montero, E. & Contini, T. 2009, MNRAS, 398, 949
Pérez-Montero, E., Contini, T., Lamareille, F., et al. 2013, A&A, 549, A25
Pérez-González, P. G., Rieke, G. H., Villar, V., et al. 2008, ApJ, 675, 234

Sánchez Almeida, J., Morales-Luis, A. B., et al. 2014, ApJ, 783, 45
Tasca, L. A. M., Kneib, J.-P., Iovino, A., et al. 2009, A&A, 503, 379
Troncoso, P., Maiolino, R., Sommariva, V., et al. 2014, A&A, 563, A58
van der Wel, A., Straughn, A. N., Rix, H.-W., et al. 2011, ApJ, 742, 111
Whitaker, K. E., van Dokkum, P. G., Brammer, G., & Franx, M. 2012, ApJ, 754, L29
Yan, R., Ho, L. C., Newman, J. A., et al. 2011, ApJ, 728, 38
Zahid, H. J., Kewley, L. J., & Bresolin, F. 2011, ApJ, 730, 137

[1] INAF–Osservatorio Astronomico di Roma, via di Frascati 33, I-00040, Monte Porzio Catone, Italy
[2] Aix Marseille Université, CNRS, LAM (Laboratoire d'Astrophysique de Marseille) UMR 7326, 13388, Marseille, France
[3] INAF–Osservatorio Astronomico di Bologna, via Ranzani,1, I-40127, Bologna, Italy
[4] INAF–IASF, via Bassini 15, I-20133, Milano, Italy
[5] University of Bologna, Department of Physics and Astronomy (DIFA), V.le Berti Pichat, 6/2 - 40127, Bologna
[6] INAF–IASF Bologna, via Gobetti 101, I–40129, Bologna, Italy
[7] Institut d'Astrophysique de Paris, UMR7095 CNRS, Université Pierre et Marie Curie, 98 bis Boulevard Arago, 75014 Paris, France
[8] Institut de Recherche en Astrophysique et Planétologie - IRAP, CNRS, Universit de Toulouse, UPS-OMP, 14, avenue E. Belin, F31400 Toulouse, France
[9] Department of Astronomy, University of Geneva ch. d'cogia 16, CH-1290 Versoix
[10] Geneva Observatory, University of Geneva, ch. des Maillettes 51, CH-1290 Versoix, Switzerland
[11] Centro de Estudios de Física del Cosmos de Aragón, Teruel, Spain
[12] Caltech, Pasadena, USA
[13] University of Massachussetts
[14] Max-Planck-Institut für Extraterrestrische Physik, Postfach 1312, D-85741, Garching bei München, Germany
[15] Research Center for Space and Cosmic Evolution, Ehime University, Bunkyo-cho 2-5, Matsuyama 790-8577, Japan

Table 2. Derived physical properties of EELGs in VUDS

VUDS ID	RA	DEC	z	I_{AB}	$M_{AB}(B)$	$\log M_\star$	$\log SFR_{H\alpha,H\beta}$	$12+\log(O/H)$
	deg(*J*2000)	*deg*(*J*2000)		*mag*	*mag*	$M_\odot$	$M_\odot yr^{-1}$	
(1)	(2)	(3)	(4)	(5)	(6)	(7)	(8)	(9)
520276545	36.288532	-4.500415	0.8614	24.895	-17.9	$8.4^{+0.55}_{-0.47}$	-0.17 ±0.24	8.06 ±0.17
520281627	36.33267	-4.492811	0.4033	23.589	-17.3	$8.0^{+0.34}_{-0.06}$	-0.78 ±0.11	8.21 ±0.07
520290391	36.390442	-4.476896	0.7411	24.928	-17.5	$8.04^{+0.35}_{-0.27}$	-0.18 ±0.16	7.79 ±0.08
520246239	36.485642	-4.552226	0.6177	24.244	-17.7	$7.97^{+0.2}_{-0.27}$	-0.41 ±0.15	8.22 ±0.13
520327062	36.592604	-4.414382	0.7065	23.929	-18.2	$8.09^{+0.02}_{-0.0}$	-0.21 ±0.09	7.96 ±0.16
520388031	36.617849	-4.310487	0.527	24.194	-17.1	$8.14^{+0.08}_{-0.08}$	-0.47 ±0.15	8.24 ±0.12
520420821	36.64344	-4.254594	0.555	23.537	-17.5	$7.89^{+0.04}_{-0.09}$	-0.14 ±0.06	8.03 ±0.06$^\psi$
520349673	36.66636	-4.376334	0.5183	23.623	-17.8	$8.33^{+0.16}_{-0.0}$	-0.57 ±0.07	7.79 ±0.17$^\psi$
520316717	36.719163	-4.432611	0.6935	24.213	-18.1	$8.43^{+0.12}_{-0.01}$	-0.27 ±0.04	7.96 ±0.06
520433508	36.78282	-4.230942	0.8464	24.777	-18.0	$8.26^{+0.05}_{-0.08}$	-0.21 ±0.13	8.06 ±0.2
520344687	36.813187	-4.38421	0.8011	24.974	-17.6	$8.06^{+0.25}_{-0.21}$	-0.18 ±0.17	7.92 ±0.21
530076899	52.981115	-27.583964	0.34	25.388	-15.6	$7.46^{+0.15}_{-0.21}$	-1.61 ±0.03	8.05 ±0.19
530076254	53.056834	-27.588217	0.25	24.545	-15.1	$7.55^{+0.53}_{-0.28}$	-1.42 ±0.21	8.32 ±0.16
530080539	53.062864	-27.560883	0.84	24.426	-18.8	$8.6^{+0.23}_{-0.4}$	0.11 ±0.12	8.29 ±0.16
530053182	53.065926	-27.730899	0.375	24.33	-16.5	$7.08^{+0.26}_{-0.17}$	-0.27 ±0.04	7.66 ±0.04$^\psi$
530046029	53.085412	-27.772514	0.67	24.577	-17.3	$7.82^{+0.53}_{-0.24}$	-0.48 ±0.15	8.3 ±0.23
530048721	53.168253	-27.756505	0.57	25.186	-16.7	$7.76^{+0.18}_{-0.09}$	-0.92 ±0.05	7.97 ±0.27
530043711	53.245908	-27.786269	0.62	24.136	-18.1	$8.15^{+0.25}_{-0.22}$	-0.12 ±0.07	8.34 ±0.12
530079125	53.256513	-27.569361	0.38	25.204	-15.9	$7.27^{+0.81}_{-0.23}$	-1.19 ±0.12	7.86 ±0.1
510830468	149.78862	2.031251	0.6745	24.302	-17.0	$7.5^{+0.08}_{-0.09}$	0.23 ±0.08	7.58 ±0.07$^\psi$
510146174	149.790243	1.988252	0.4781	24.995	-15.6	$7.18^{+0.24}_{-0.3}$	-1.18 ±0.21	7.8 ±0.24
511475480	149.92956	2.565804	0.6634	24.336	-16.7	$7.45^{+0.12}_{-0.09}$	-0.11 ±0.14	7.55 ±0.08$^\psi$
510573089	149.93424	1.937292	0.5472	23.331	-17.9	$7.95^{+0.55}_{-0.17}$	-0.08 ±0.15	8.01 ±0.06$^\psi$
510809459	149.96752	2.00106	0.6614	24.449	-17.2	$7.99^{+0.11}_{-0.03}$	-0.93 ±0.12	7.78 ±0.11
510352169	149.99831	1.786842	0.6282	23.792	-17.4	$7.51^{+0.22}_{-0.08}$	0.04 ±0.08	7.62 ±0.04
510229076	150.049327	2.137676	0.2197	24.867	-14.5	$6.9^{+0.12}_{-0.12}$	-1.38 ±0.18	8.04 ±0.15
510997797	150.08421	2.266334	0.2837	24.547	-15.2	$7.33^{+0.18}_{-0.18}$	-1.1 ±0.14	8.23 ±0.2
510175664	150.113065	2.042952	0.5018	24.976	-15.9	$7.67^{+0.3}_{-0.17}$	-0.48 ±0.21	7.77 ±0.23
5120568170	150.177749	1.803126	0.3389	24.977	-15.2	$7.65^{+0.45}_{-0.58}$	-1.5 ±0.26	8.21 ±0.24
5101659094	150.32707	2.647341	0.6782	24.18	-17.9	$8.29^{+0.07}_{-0.05}$	-0.81 ±0.16	8.19 ±0.22
5101657178	150.38803	2.660747	0.5633	24.232	-17.4	$7.86^{+0.1}_{-0.06}$	-0.59 ±0.08	7.76 ±0.11$^\psi$

Notes: (a) metallicity derived through the direct method. (1) VUDS ID; (2) and (3) Right ascension and declination (J2000); (4) Spectroscopic redshift; (5) (6) Rest-frame absolute B-band magnitude; (7) and (8) Stellar mass from SED fitting and star formation rate from Hα or Hβ luminosity (Chabrier (2003) IMF); (9) Gas-phase metallicity through the *R23* calibration (McGaugh 1991) scaled to the direct method using the linear relation detailed in Lamareille et al. (2006). Those entries with ψ indicate metallicities derived through the direct (T_e) method (Hägele et al. 2008). (The entire version of this table for the full sample of galaxies is available *On-line*).